Free, Stable Continental Shelf Waves in a Sheared, Barotropic Boundary Current[1]

DAVID A. BROOKS[2] AND CHRISTOPHER N. K. MOOERS[3]

University of Miami Rosenstiel School of Marine and Atmospheric Science, Miami, Fla. 33149

(Manuscript received 21 July 1976, in revised form 4 February 1977)

ABSTRACT

The dispersion characteristics of stable, discrete, barotropic, continental shelf wave (CSW) modes propagating in a barotropic boundary current are strongly modified by the dynamical effects of nonuniform horizontal shear. For example, the CSW's propagate *cum sole* with no mean current, but their direction of propagation can be reversed by an opposing uniform mean current. In contrast, an opposing sheared mean current increases the tendency for *cum sole* propagation relative to an opposing uniform mean current, and produces a high-wavenumber cutoff, at least for modes higher than the first. If the sheared mean flow vanishes somewhere, the discrete CSW modes all propagate *cum sole* once again. For the mean current profiles considered, the high-frequency cutoff is lowered in the nonuniform shear case compared to the zero current case.

In a simple geometry motivated by the Florida Current and Florida Straits, southward CSW propagation can occur, in opposition to the Current, primarily because the cyclonic shear of the Current is similar in magnitude to the local Coriolis parameter. The short-period cutoff (zero group speed) for the first mode CSW is about 12 days; this CSW has a wavelength of about 190 km, corresponding to a southward phase speed of about 17 cm s^{-1}. Within the limitations of the model, the results indicate that the Florida Straits–Florida Current system can accumulate energy at time scales of 10–14 days, corresponding to those of atmospheric cold front forcing.

1. Introduction and motivation

Pillsbury (1890) noted that the Florida Current was perturbed by atmospheric disturbances. Recently, evidence for atmospheric forcing of the Florida Current's fluctuations has been more fully documented by Mooers and Brooks (1977), Brooks and Mooers (1977) and Düing *et al.* (1977). Hamon (1962) observed sea level disturbances propagating along the Australian coasts which were correlated with atmospheric forces. Robinson (1964) interpreted these motions as topographically trapped (continental shelf) waves (CSW's) generated by atmospheric forces.

Present theories do not explain how an intense, sheared mean current modifies CSW's. This shortcoming is particularly serious in western boundary currents because the wave phase velocities of stable CSW's and the current velocity are of the same order of magnitude but opposed in direction. Furthermore, the horizontal velocity shear in a western boundary current can be similar in magnitude to the Coriolis parameter; and it contributes to the mean potential vorticity, whose variation provides the restoring force for CSW's.

Mysak (1967) considered the effects of an "offshelf," uniform mean current on CSW propagation. For mean current values typical of the East Australian Current, he found reasonable agreement between the theoretical lowest mode phase speed and the propagation speed of sea level disturbances calculated by Hamon (1962). However, the model mean current had no horizontal shear and was located over a flat bottom offshore, where the wave motion is evanescent.

More general CSW problems have been addressed. For example, Wang (1975) employed a two-layer model without a mean current; he found a "resonance interaction" between the baroclinic Kelvin wave and the lowest CSW mode in strongly stratified cases. In a subsequent paper, Wang and Mooers (1976) included continuous stratification without a mean current, and found that CSW wave speeds were increased somewhat compared to the barotropic case. Niiler and Mysak (1971) considered a barotropic model with discontinuous mean current and depth profiles. They found that relatively long CSW's could travel along the shelf in both directions, and that the short waves could only travel northward and were unstable for certain short wavelengths. Here we investigate the importance of a barotropic mean cur-

[1] Contribution from the Rosenstiel School of Marine and Atmospheric Science.

[2] Present affiliation: Department of Geosciences, North Carolina State University, Raleigh, N. C. 27607.

[3] Present affiliation: College of Marine Studies, University of Delaware, Lewes 19958.

rent with nonuniform but continuous horizontal shear, and a continuous depth profile, on the dispersion characteristics of stable CSW's. As explained later, unstable wave solutions have been deliberately excluded through choice of methodology. The motivation for this study is drawn from the Florida Straits–Florida Current system, of which our model is an approximation. A discriminant analysis for the governing equation sets bounds on CSW phase speeds and provides a qualitative check on numerical solutions. In order to focus on the effects of a sheared mean current, a case in which the bottom topography does not contribute to the variable part of the wave restoring force is presented. Finally, a general case in which both the depth and mean current profiles provide restoring forces dependent on the cross-shelf coordinate is examined. The relevance of the results to the actual Florida Current–Florida Straits system is discussed in the Appendix.

2. The model equations

We consider an infinitely long, north–south (y) channel in the Northern Hemisphere with depth h and a sheared, barotropic northward mean current V (Fig. 1). The depth and the mean current are assumed to vary only in the cross-channel (east–west, x) direction. The latitudinal variation of the Coriolis parameter f (the "β effect") is neglected, in favor of the topographic vorticity restoring effect which is much larger in the cases considered. To nondimensionalize the variables, the following scale factors are used: the shelf width L for the horizontal coordinates, the reciprocal Coriolis parameter f^{-1} for time, the maximum water depth H for the depth profile and the geostrophic velocity scale for the horizontal velocities. The dimensionless momentum and continuity equations for small-amplitude, barotropic, nondivergent perturbations of the basic state are

$$\frac{Du}{Dt}-v=-\eta_x, \tag{1}$$

$$\frac{Dv}{Dt}+u(1+\mathrm{Ro}V_x)=-\eta_y, \tag{2}$$

$$(hu)_x+(hv)_y=0, \tag{3}$$

where (u,v,η) are the perturbation (x,y) velocity components and sea level elevation, respectively; subscripts denote partial differentiation, $D(\cdot)/Dt\equiv(\cdot)_t+\mathrm{Ro}V(\cdot)_y$; and $\mathrm{Ro}=V_{\max}/fL$ is the mean flow Rossby number, with $V_{\max}$ the maximum mean current speed. Eq. (3) permits the introduction of a mass transport streamfunction $\hat{\psi}$ such that $hu=-\hat{\psi}_y$ and $hv=\hat{\psi}_x$. We seek wave solutions of the form

$$\hat{\psi}=\psi(x)\exp[i(s_0t-\delta y)], \tag{4}$$

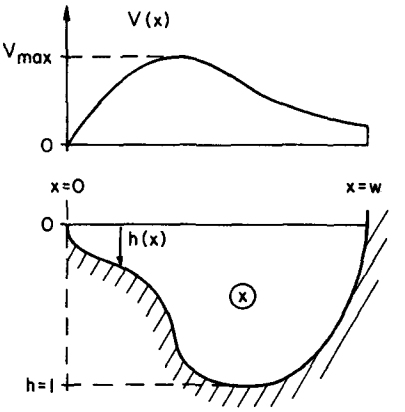

FIG. 1. The depth and mean current profiles.

where $\psi(x)$ is the cross-channel structure function and s_0 and δ are the dimensionless wave frequency and wavenumber. Then the total time derivative is $D(\cdot)/Dt=is(\cdot)$, where $s(x)=s_0-\mathrm{Ro}\delta V(x)$ is the intrinsic frequency. By definition s_0 is the wave frequency relative to the earth and s is the wave frequency relative to the mean current. The potential vorticity P of the basic state is $P=(1+\mathrm{Ro}V_x)/h$ and the depth-weighted potential vorticity gradient, hP_x, is $hP_x=\mathrm{Ro}V_{xx}-(h_x/h)(1+\mathrm{Ro}V_x)$. Cross-differentiation of (1) and (2) and substitution of (4) yields the governing equation for ψ:

$$\psi_{xx}-\frac{h_x}{h}\psi_x-\left(\delta^2-\frac{\delta}{s}hP_x\right)\psi=0. \tag{5}$$

For the channel geometry of Fig. 1, the boundary conditions are $\psi=0$ at $x=1, W$.

Analytic solutions to (5) exist only for certain simple choices of $h(x)$ and $V(x)$, e.g., an exponential dependence for h and V constant (Adams and Buchwald, 1969). We have used the numerical technique described by Lindzen and Kuo (1969) to solve (5) for general depth and mean current profiles. The solutions are obtained by searching for resonant responses driven by an arbitrarily introduced forcing term on the right-hand side of (5); for detailed examples, see Brooks (1975). [The wavenumber of the imposed forcing is prescribed to be real, and the frequency has a small damping component to allow integration of (5) over critical points. Thus, unstable waves are excluded *a priori*.] We also compared several dispersion curves obtained by the forced method with those obtained by the "shooting method" (Keller, 1969), with excellent agreement; the forced method was found to be considerably less expensive to execute, particularly in cases involving multiple waveguide interactions.

3. Discriminant analysis

The discriminant of the governing equation is used to identify the domain in which oscillatory solutions

are confined. The analysis of the discriminant locates the turning points and critical points of the governing equation and provides upper and lower bounds on the wave phase speed, $c_0=s_0/\delta$, for oscillatory solutions.

In self-adjoint form, (5) becomes

$$\left(\frac{\Psi'}{h}\right)'-\left(\delta^2-\frac{hP'}{c}\right)\frac{\Psi}{h}=0, \tag{6}$$

where $c(x)=c_0-\mathrm{Ro}V(x)$ is the intrinsic wave phase speed and primes denote differentiation in x. Conditions for turning points are discussed below. Critical point singularities occur where $c(x)$ vanishes.[4] The substitution $\psi(x)=h^{\frac{1}{2}}\phi(x)$ reduces Eq. (6) to $\phi''+\Delta\phi=0$, where the discriminant Δ is

$$\Delta=\frac{hP'}{c}-\left[\delta^2+\frac{3}{4}\left(\frac{h'}{h}\right)^2-\frac{1}{2}\frac{h''}{h}\right].$$

For a given δ and model geometry, the zeros of Δ (turning points) provide x-dependent upper and lower bounds on $c(x)$ such that ϕ and ψ are oscillatory for that range of x where $\Delta>0$. The necessary condition for oscillatory behavior is

$$\frac{hP'}{c}>\delta^2-q, \tag{7}$$

where $q\equiv(h''/2h)-\frac{3}{4}(h'/h)^2$. Of course, this condition is not sufficient to assure that a given δ allows compliance with the boundary conditions, a point which is settled when solutions to the corresponding eigenvalue problem are obtained.

Additional bounds on $c(x)$ can be obtained directly from (6), which can be written as two coupled, first-order equations: $Q'=A(x)\psi$ and $\psi'=-hQ$, where $Q(x)=-\psi'/h$ and $hA(x)=-\delta^2+hP'/c$. The functions ψ and Q oscillate in segments of the x domain where $A>0$ and $h>0$ (Eckart, 1960). Since h is positive definite, this condition is

$$\frac{hP'}{c}>\delta^2. \tag{8}$$

A comparison of (7) and (8) shows that for $q<0$, a more restrictive bound on c is given by (7). However, in regions of extreme bottom curvature, such as near the shelf edge, q may be positive; in such regions, (8) provides the more restrictive bound. There are four cases which depend upon the signs of q and P'. The least upper and greatest lower bounds on c_0 are given by

Case a. $P'<0$, $q<0$

$$\frac{hP'}{\delta^2-q}<c<0 \quad \text{or} \quad \frac{hP'}{\delta^2-q}+\mathrm{Ro}V<c_0<\mathrm{Ro}V$$

Case b. $P'<0$, $q>0$

$$\frac{hP'}{\delta^2}<c<0 \quad \text{or} \quad \frac{hP'}{\delta^2}+\mathrm{Ro}V<c_0<\mathrm{Ro}V$$

Case c. $P'>0$, $q<0$

$$0<c<\frac{hP'}{\delta^2-q} \quad \text{or} \quad \mathrm{Ro}V<c_0<\frac{hP'}{\delta^2-q}+\mathrm{Ro}V$$

Case d. $P'>0$, $q>0$

$$0<c<\frac{hP'}{\delta^2} \quad \text{or} \quad \mathrm{Ro}V<c_0<\frac{hP'}{\delta^2}+\mathrm{Ro}V.$$

As $|\delta|\to\infty$, c_0 is bounded from above and below by RoV, i.e., very short waves advect with the mean current. As $|\delta|\to 0$, c_0 is unbounded from below if $P'<0$ and $q\gtrless 0$, and c_0 is unbounded from above if $P'>0$ and $q\gtrless 0$. For monotonically increasing depth, $h'\gtrless 0$, Grimshaw (1976) proved that $c_0\lesssim\min(V(x))$ and P must be negative somewhere for neutral modes (CSW's) to exist; the results of the next section are perfectly consistent with these statements. Such strong statements are not available for the non-monotonic depth to be eventually treated here.

4. The exponential shelf with a sheared mean current

An exponential shelf model is chosen to facilitate the analysis of the effects of a nonuniformly sheared mean current. The depth equation used for these calculations is

$$h=\begin{cases} h_0e^{2bx}, & 0\lesssim x\lesssim 1 \\ 1, & 1<x\lesssim W \end{cases} \tag{9}$$

with the parameters $h_0=0.625$, $b=1.385$ and $W=2.5$ suggested by the Florida Straits geometry; hence, $q=-b^2$. An exponential model for the mean current profile is also employed, $\mathrm{Ro}V(x)=\mathrm{Ro}xe^{(1-x)}$, which has a maximum at $x=1$, an inflection point at $x=2$ and vanishes at $x=0$ and as $x\to\infty$. Fig. 2 shows RoV, h, P, P' and hP' for the exponential shelf and mean

[4] Critical surfaces (vertical planes parallel to the current axis where c vanishes) exist for waves propagating along *and* across a mean barotropic current. In the depth-integrated form, the system (1)–(3), the critical surfaces become critical lines parallel to the current axis. For waves which only propagate along the current, the critical lines become critical points. These waves must satisfy two-point boundary conditions in x and are thus normal modes or eigensolutions if they exist. For Rossby waves in a barotropic atmosphere, Dickinson (1968) found that propagating waves are absorbed at and near critical planes, which eliminates the possibility for the existence of discrete, stable normal modes when c_0 equals $V(x)$ for some x. McKee (1977) has recently demonstrated that a continuous spectrum for c_0 exists between the minimum and maximum values of $V(x)$. The corresponding solutions have discontinuous derivatives at critical points.

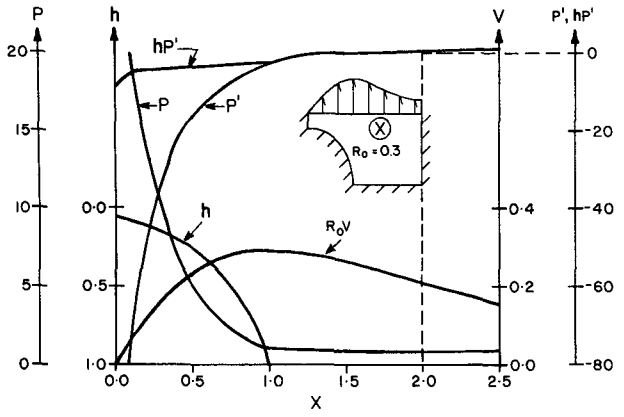

FIG. 2. Cross-channel distributions of h, RoV, P, P_x and hP_x for the exponential shelf-exponential mean current model shown in the inset.

current model, with Ro=0.3. For $x<2$, $P'<0$; thus Case a of the previous section applies, and the intrinsic phase speed is upstream.

Fig. 3 shows two "discriminant diagrams" for the exponential shelf-exponential mean current model. These diagrams illustrate the phase speed constraints as a function of x. The mean current profile RoV shown by the dashed line for the case Ro=0.3, provides the upper bound for the phase speed of waves trapped over the shelf. The solid line in Fig. 3a shows the lower phase speed bound for $\delta=-1$. The region in which oscillatory solutions can exist for $\delta=-1$ is shaded. Three distinct possibilities are shown in panel A by the horizontal lines labeled A, B and C. The circles indicate turning points, and the triangles indicate critical points. Line A shows the case of a southward wave with oscillatory behavior for $0\leqslant x\leqslant 1.0$, and an evanescent behavior for $x>1.0$. Lines B and C show cases in which northward waves have one and two critical points, respectively.

Fig. 3b shows analogous results for several δ's. It can be seen that all northward waves have critical points, and that the oscillatory domain of southward waves with wavelengths $\lesssim 65$ km ($|\delta|>2.9$) is confined to the shelf. In the short-wave limit, southward waves become stationary ($c_0\to 0$) and compressed into a vanishingly small strip adjacent to the cyclonic boundary.

From solutions to (5), four dispersion diagrams have been constructed (Fig. 4) for the exponential shelf model. Positive (negative) s_0 corresponds to southward (northward) phase propagation. The shear of the mean flow increases from zero in Figs. 4a–4d. In each case Ro has been adjusted to maintain a fixed total transport. The two lowest order shelf modes are shown. A uniform flow (Fig. 4a) transforms the zero-flow dispersion diagram kinematically according to $\delta'=\delta$, $s_0'=s_0-\mathrm{Ro}|\delta|V$, where primes denote the transformed system (not simply a rotation of axes). The uniform flow permits downstream propagation,

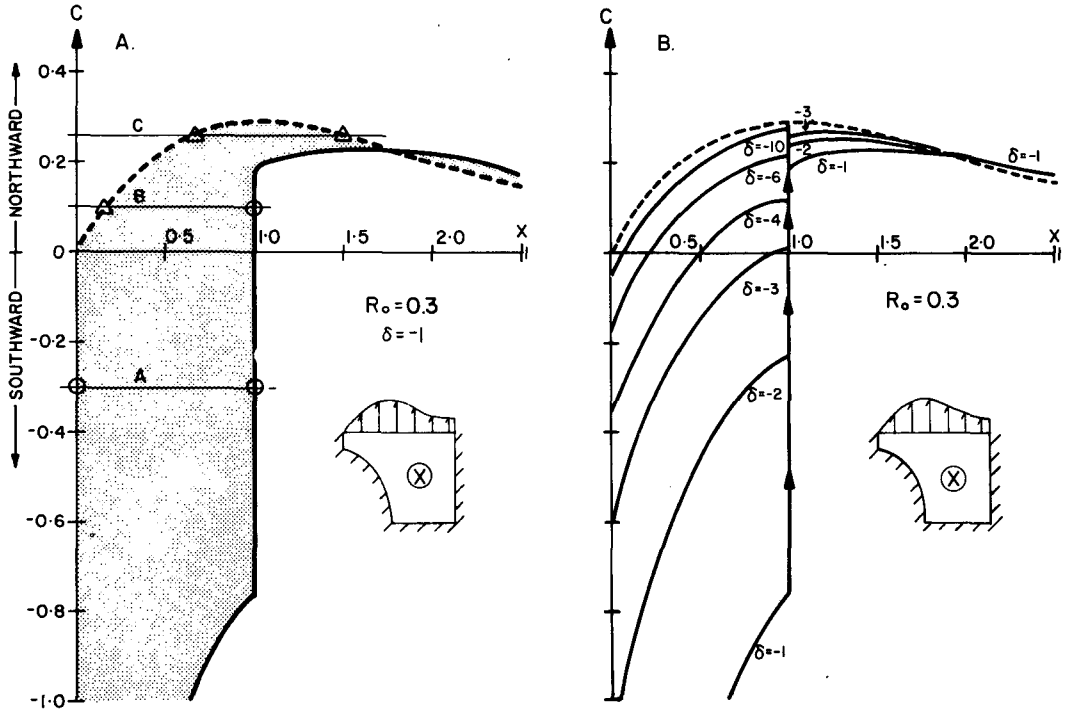

FIG. 3. Discriminant diagrams for the exponential shelf-exponential mean current model: (A) $\delta=-1$, shaded area is oscillatory domain, circles (triangles) indicate turning (critical) points for selected c_0; (B) For selected δ, the oscillatory domain is bounded by the dashed curve and the corresponding solid curve.

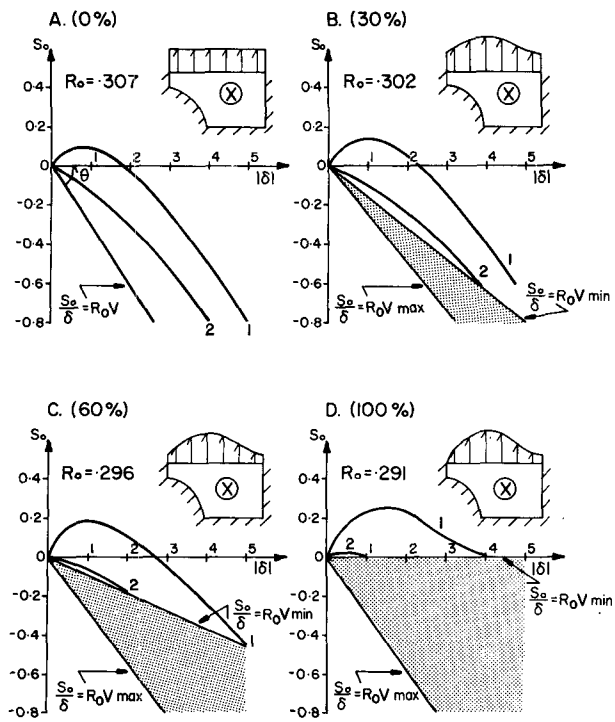

FIG. 4. Dispersion curves for modes 1 and 2 for the exponential shelf model, showing the effect of gradually transforming the uniform current profile of panel A into the damped exponential current profile of panel D. The total transport is 30×10^6 m^3 s^{-1} in all cases. The shaded areas show the zones of singular points in the governing equation. The velocity profile is given by RoV, where $V=0.78+A(xe^{(1-x)}-0.78)$. Parameter A (given in percent) is shown in parentheses.

provided $c_0\leqslant \mathrm{Ro}V$. This bound is shown in Fig. 4a by the line with slope equal to RoV. There are no critical points,[5] so the dispersion curves extend to indefinitely large wavenumbers. As the current shear is increased, the boundary line $s_0=\mathrm{Ro}\delta V$ in Fig. 4a expands into a wedge in Figs. 4b–4d bounded by the lines $(s_0)_1=\mathrm{Ro}\delta V_{\min}$ and $(s_0)_2=\mathrm{Ro}\delta V_{\max}$, where $V_{\min}$ and $V_{\max}$ are the minimum and maximum values of V. For all points inside the wedge, one or two critical points occur somewhere in the channel. The dispersion curves for stable, discrete modes lie outside the wedge and terminate at the wedge boundary. If the mean flow is zero anywhere in the channel, then the wedge completely fills the northward half of the dispersion diagram, as in Fig. 4d; and stable, discrete downstream modes cannot exist.

5. A general case

We consider a simple model in which the topographic terms in the discriminant are x-dependent. Our motivation is drawn from the Florida Straits–Florida Current system, which has a channel-like geometry with an inshore Terrace and a steep offshore slope. The Miami Terrace is part of a CSW waveguide that extends southward from at least Cape Hatteras to at least the Florida Keys. The waveguide length is more than 50 times its width at the Miami Terrace.

We employ a polynomial function fitted to the depth profile off Miami, and we retain the exponential current profile to represent the vertically averaged Florida Current. With Ro=0.444, the total (dimensional) volume transport is 30×10^6 m^3 s^{-1}, a typical value for the Miami–Bimini section (Niiler and Richardson, 1973). Fig. 5 shows the corresponding profiles for h, P and hP'.

a. No mean current

For case Ro=0, the Miami Terrace has two waveguides for southward waves, and the Bimini shelf has a single waveguide for northward waves (Fig. 6). Modes 1 and 2 (Fig. 7a) are influenced by a "resonance interaction" (Eckart, 1962) between the lowest mode computed individually for each Terrace waveguide (Fig. 7b). (The individual waveguide dispersion curves were computed for "upper slope" ($0\leqslant x\leqslant 0.56$) and "lower slope" ($0.56\leqslant x\leqslant 1.31$) segments of the bottom profile; the bottom was flat for other x values.) As a consequence of the interaction, mode 1 has a small group speed for a very broad band of wavenumbers. The interaction is strongest at a dimensional wavelength of about 40 km, i.e., the order of the shelf width. For longer wavelengths, modes 1 and 2 span both the upper and lower slopes; for shorter wavelengths, mode 1 is associated with the upper slope and mode 2 with the lower slope.

b. Sheared mean current

For $|\delta|\gtrsim 3$, the lower slope waveguide ceases to exist for southward waves (Fig. 8). The upper slope

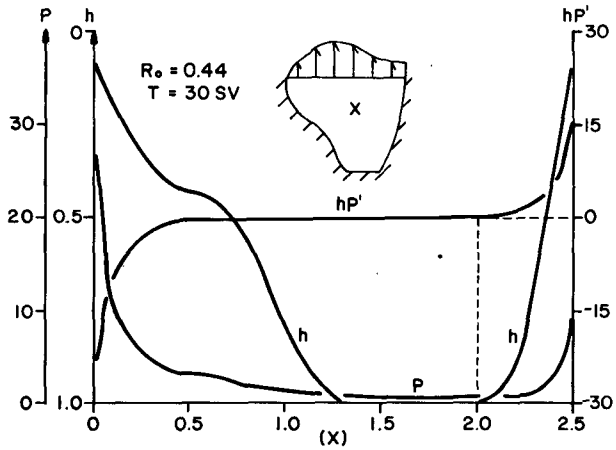

FIG. 5. Cross-channel distribution of h, P and hP_x for the terraced (polynomial) channel-exponential mean current model.

[5] Actually, the line $s_0=\mathrm{Ro}\delta V$ is a channel-wide critical "point," analogous to $s_0=0$ in the zero mean flow case.

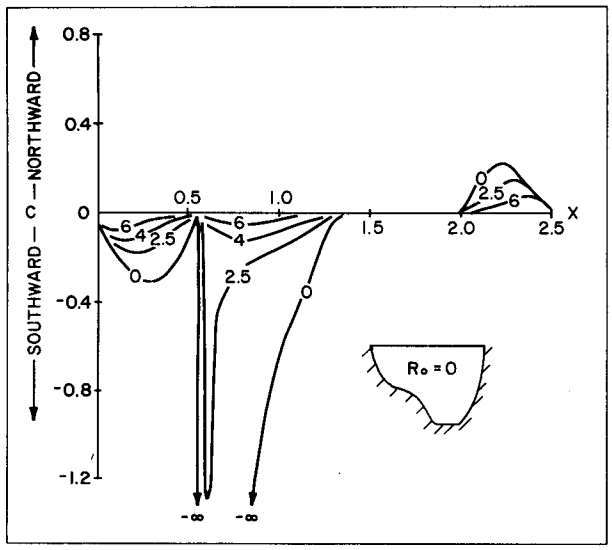

FIG. 6. Discriminant diagram for the terraced channel model, Ro=0.

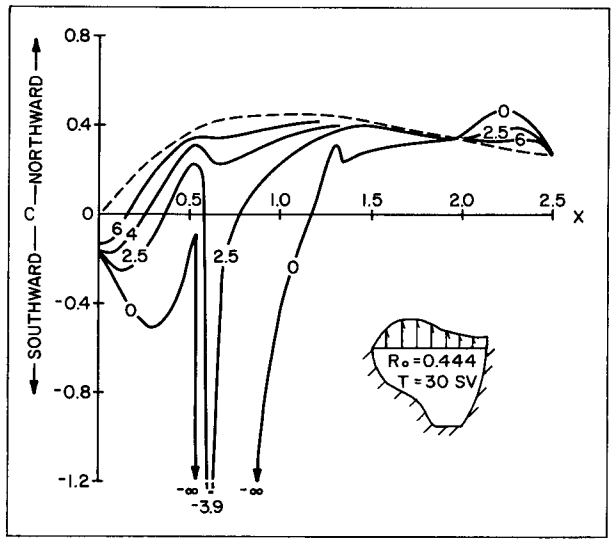

FIG. 8. Discriminant diagram for the terraced channel-exponential mean current model, Ro=0.444.

waveguide provides a southward potential for all wavelengths, but the propagation zone is compressed into a narrow band near the boundary for short wavelengths.

Fig. 9 shows first and second mode dispersion curves for sheared (solid lines) and uniform (dashed lines) mean current cases. The total integrated transport is 30×10^6 m^3 s^{-1} in both cases. The large phase speed differences between the cases occur because the uniform mean current model does not incorporate the dynamic effects of nonuniform current shear. Our dispersion curve for the gravest southward CSW mode in the sheared current is similar for small wavenumbers to that shown by Niiler and Mysak (1971) for their model of the Gulf Stream in the Blake Plateau region. However, we find no high-wavenumber cutoff for the gravest southward mode, because high-

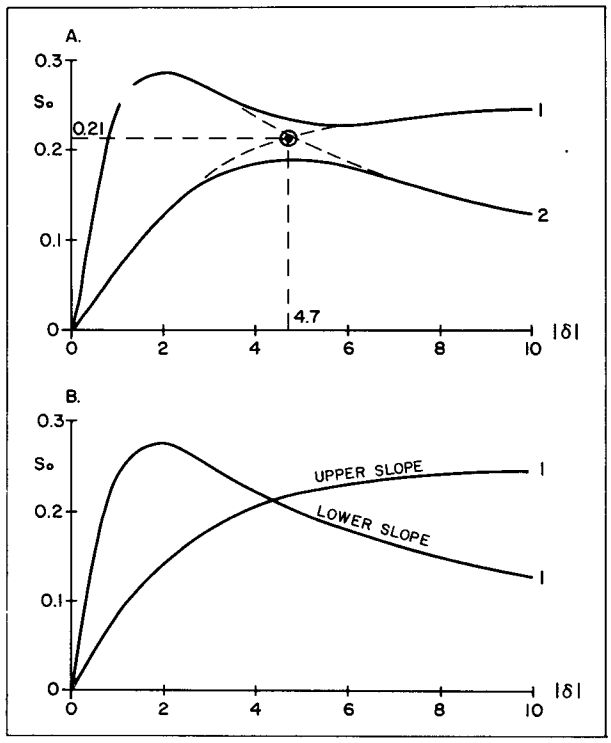

FIG. 7. Dispersion diagrams for the terraced channel, Ro=0. (A) The two lowest order modes for the full channel; (B) the first modes for the upper slope and lower slope only channels.

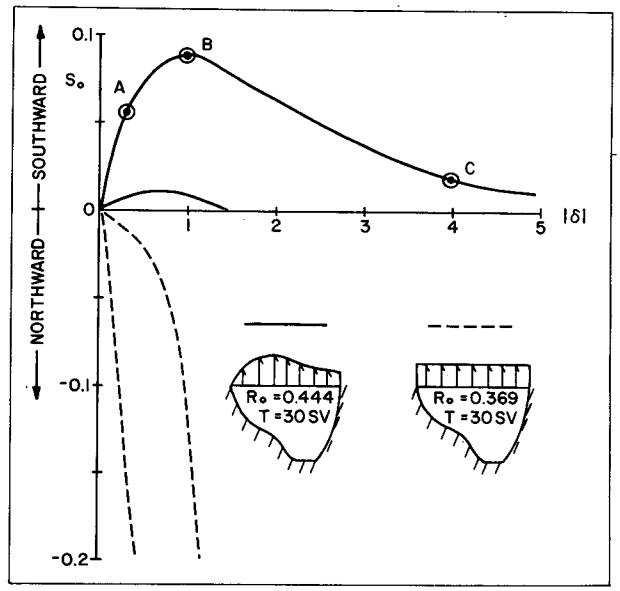

FIG. 9. Dispersion diagram for the terraced channel model: (solid line) exponential mean flow, Ro=0.444; (dashed line) uniform mean flow, Ro=0.369. The total transport is 30×10^6 m^3 s^{-1} in both cases. Encircled points refer to cases in Fig. 10.

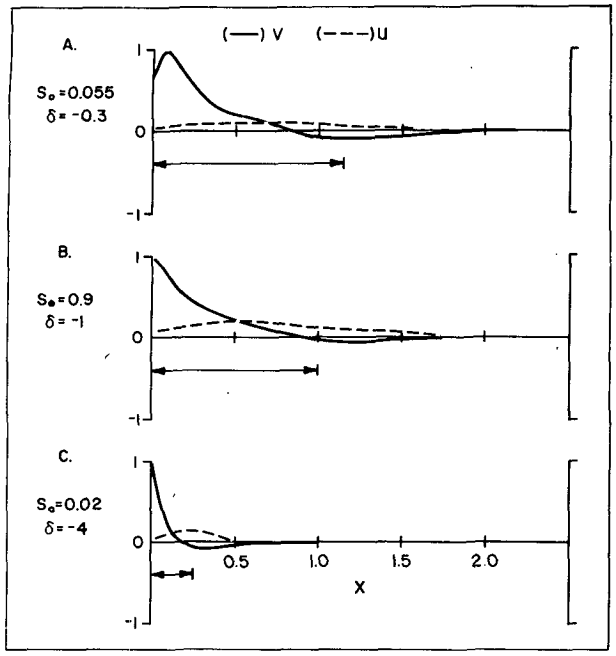

FIG. 10. Cross-stream structure functions for the terraced channel-exponential mean current model, Ro=0.444. Cases correspond to the encircled points on Fig. 9.

wavenumber CSW's are trapped very close to the cyclonic boundary where the kinematic effect of the mean current is relatively small. Second and higher order southward modes do experience high-wavenumber cutoffs. Stable, discrete CSW modes were not found for downstream propagation in the sheared mean current.

The first mode cross-stream eigenfunctions at the (s_0,δ) points encircled in Fig. 9 confirm that for $|\delta|>3.0$, the wave is trapped in a narrow zone near the western boundary (Fig. 10c). The horizontal arrows in Fig. 10 show the range of the oscillatory domain of the eigenfunctions, determined independently from the discriminant diagram (Fig. 8). The waves are evanescent outside this domain. The eigenfunctions of Figs. 8a and 8b were computed for a "long" (nearly nondispersive) wave and the zero group speed wave, respectively. For all cases, the wave is effectively trapped over the Miami Terrace. For the zero group speed wave, the maximum alongshore velocity component (v) occurs adjacent to the western boundary, a node in the v component occurs about 30 km offshore (~10 km seaward of the Terrace edge), and the maximum cross-shelf velocity component (u) occurs near the Terrace edge and is about 20% of the maximum v.

To estimate the sensitivity of the Miami Terrace CSW characteristics to the Grand Bahama Bank, the dispersion curves were computed with the Bimini slope removed, i.e., the bottom was flat for $x>1.3$. The exponential current profile was retained, with Ro =0.444 as before. The dispersion curves (not shown) were virtually indistinguishable from those of Fig. 9, within the resolution of the calculations ($\Delta s_0=0.01$), and over the wavenumber range $0\leqslant|\delta|\leqslant 5$. We conclude that the Bahama Bank has a negligible effect on the characteristics of southward shelf waves trapped over the Miami Terrace.

6. Summary

Particularly in western boundary currents, the contribution of the mean shear to the mean potential vorticity can significantly influence the dispersion characteristics of CSW's. For CSW's propagating *cum sole* and in opposition to the mean current, the high-frequency cutoff is lowered from the zero mean current case, and a high-wavenumber cutoff can occur, an effect which increases with mode number. The subinertial frequency, southward propagating disturbances observed along the east Florida coast and the Florida Keys (Brooks and Mooers, 1977) apparently occur because the cyclonic shear of the Florida Current approaches the magnitude of the Coriolis parameter, thereby providing a southward CSW tendency sufficient to overcome northward advection by the mean Current. In a model with a uniform mean current carrying the same transport CSW's are advected northward.

The barotropic model indicates that the gravest mode CSW of the Florida Straits–Florida Current system has low group speed at periods of 10–14 days and wavelengths of 180–200 km. Thus a vigorous response might be expected for southward propagating atmospheric disturbances with these time and space scales, such as atmospheric cold fronts, for example. However, the limitations of the model may be severe; in particular, the baroclinic structure of the Florida Current may play a substantial role in determining the topographically trapped wave characteristics (cf. the Appendix).

APPENDIX

Applicability of the Barotropic Model to the Florida Straits–Florida Current System

The model results indicate the sensitivity of CSW characteristics to the nonuniform horizontal shear of mean currents, such as western boundary currents. Our model was suggested by the geometry of the Florida Straits and Florida Current; we found it expedient to consider a barotropic analog of the baroclinic Florida Current.

The importance of vertical density stratification to coastally trapped waves has been studied by Wang and Mooers (1976) in a terraced model without a mean current. They showed that barotropic CSW's are a special case of coastally trapped waves (CTW's) occurring in the limit of vanishing stratification parameter S,

defined as $S \equiv N_{max} H_T / fL$, where N_{max} is the maximum Brünt-Väisälä frequency over the shelf, H_T the maximum shelf depth, f the Coriolis parameter and L the shelf width. For the Miami Terrace, $H_T \approx 250$ m, $L \approx 30$ km, $N_{max} \approx 10^{-2}$ rad s^{-1} and $f \approx 0.7 \times 10^{-4}$ rad s^{-1}; thus $S \approx 1$. Wang and Mooers' Fig. 2 shows that, for $S=1$ (an "intermediate" stratification case), the first mode CTW phase speed is greater than the first mode CSW phase speed. For wavelengths of the order of 200 km, the increase due to stratification is about 20%. The first mode CTW's have a predominantly barotropic alongshore velocity structure with wavelengths $\gtrsim 300$ km, particularly inshore of the shelf edge. Thus, for wavelengths much greater than the shelf width (~ 30 km), the barotropic model qualitatively reproduces the major features of the vertically stratified model. It is not clear how the addition of a baroclinic mean current will affect this result. A more complete treatment would also include the alongshore variability of the bottom topography and coastline, and address the mechanism for the setup of CTW's, taking into account critical surface phenomena and unstable wave modes.

Discussion of Wind-Forced Barotropic CSW's in the Florida Current

From an analysis of atmospheric cold fronts passing over the Straits in a 10-year period, the mean southward speed of frontal advance was 10 m s^{-1}, with a standard deviation of 4 m s^{-1} (Brooks, 1975). The mean interval between frontal passages over the Straits was 7 days, but the distribution was almost uniform between 4 and 12 days. The duration of the frontal disturbance was typically 1 day. The fastest (southward) first mode phase speed, which occurs in the long wave limit, is about 50 cm s^{-1}. Thus, the average cold front travels too fast to provide a "phase-locked" forcing of CSW's in the Straits. From Fig. 9, the dimensional southward phase speed of the zero group speed first mode wave (point B) is 17 cm s^{-1}, corresponding to a wave period of 12 days and a wavelength of 190 km.

Because of the quasi-periodic pulse nature of the frontal disturbances, the frequency spectrum of atmospheric forcing is broadbanded in the period range of 2 days to 2 weeks. Similarly, it can be expected that the north–south wavenumber spectrum of these propagating disturbances is broadbanded in the wavelength band of several hundred to several thousand kilometers. Thus, the atmospheric forcing spectrum probably has some energy near the (s_0, δ) for the zero group speed CSW. Since energy transferred to the system at the zero group speed frequency is only advected with the mean current, the Florida Straits–Florida Current system may accumulate energy at frontal forcing time scales of 10–14 days and wavelengths of 180–200 km.

Southward propagating sea level disturbances with approximately the period of the zero group speed, first mode CSW were found in the wintertime tide gage records from the Florida east coast and Florida Keys (Brooks and Mooers, 1977). The central wavelength estimate inferred from phase difference calculations was 700 km, somewhat larger than that predicted here for the zero group speed wave.[6] The sea level disturbances were coherent with both the along- and cross-isobath Miami wind stress components.

From an array of current meters moored along the 300 m isobath in the Straits, Schott and Düing (1976) concluded that the dominant subinertial frequency motion occurred at periods of 10–13 days and with a wavelength of 170 km. The phase speed was southward at 17 cm s^{-1}, the current vector rotation was anticyclonic, and the amplitude of the alongshore current fluctuation was 14 cm s^{-1}. The 300 m isobath corresponds to $x=0.68$ in our Fig. 10. Our calculations indicate that their current meters were located 7–8 km inshore of the node of the zero group speed wave, in an anticyclonic rotation zone, near the u component antinode, where the v-component magnitude is about one-third of its maximum value.

In a forced wave calculation for the model discussed here, Brooks (1975) used (frequency and wavenumber) Fourier representations of the wind stress and wind stress curl which corresponded to winter atmospheric cold fronts. The frequency spectrum of forced CSW's had a dominant peak in the 10–12 day period range, corresponding to the zero group speed, first mode CSW. The wind stress curl was found to be important both in determining the amplitude of the response, and the shape of the horizontal kinetic energy spectrum.

The alongshore barotropic current obtained by superimposing a 10-day period, first-mode barotropic CSW on the exponential mean current profile is shown in Fig. 11. The ordinate is distance offshore from Miami (the total channel width is 75 km). The wavelength corresponding to a 10-day period is about 180 km. Maximum alongshore CSW current fluctuations, which occur adjacent to the western boundary, are 14 and 28 cm s^{-1} in Figs. 11a and 11b, respectively. The amplitudes were determined from the forced model with alongshore wind stress maxima of 3 and 6 dyn cm^{-2}, respectively, which are typical for winter atmospheric cold fronts in the area. The cross-channel CSW eigenfunction is essentially that shown in Fig. 10b. We note the following features:

1) When perturbed by the CSW, the Current exhibits a meander pattern, with the Current's axis displaced a maximum of about 5 km (Fig. 11a).

2) Transient Current reversals (i.e., southward flow) occur near the western (Miami) boundary.

[6] It is likely that the tide gage array overestimated the actual along-isobath scale because the coastline is strongly curved south of Miami.

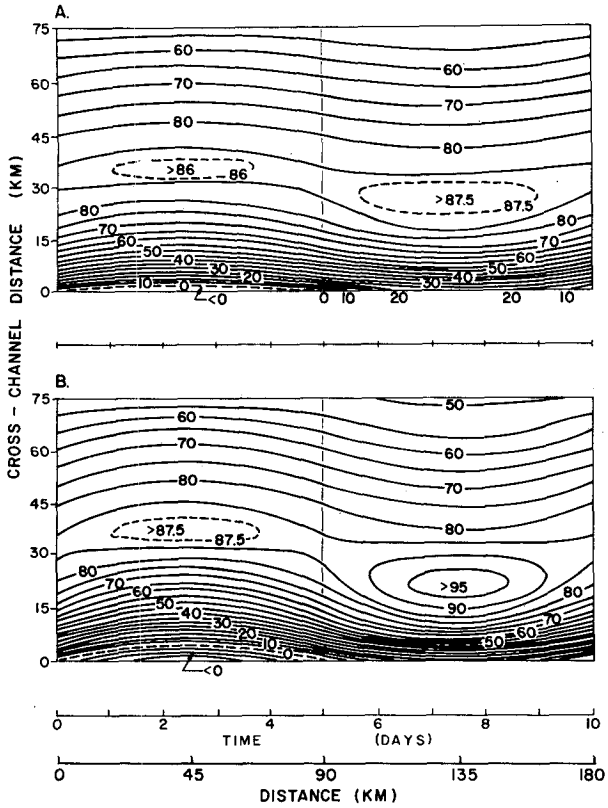

FIG. 11. Contours of the total downstream velocity (cm s^{-1}) for the terraced channel, exponential mean current model (Fig. 9). The maximum velocity for the wave component is (A) 14 cm s^{-1} and (B) 28 cm s^{-1}.

3) A node occurs in the alongshore Current fluctuation approximately 30 km offshore, near the steepest part of the Terrace topography.

4) The southward CSW has a relatively slight effect on the Current over the Bimini shelf.

Acknowledgments. This work was supported by ONR Contract N00014-67-A0201-0013 and NSF Grant DES 72-0147 AO3.

REFERENCES

Adams, J. K., and V. T. Buchwald, 1969: The generation of continental shelf waves. *J. Fluid Mech.*, **35**, 815–826.

Brooks, D. A., 1975: Wind-forced continental shelf waves in the Florida Current. Ph.D. dissertation, University of Miami, 268 pp.

——, and C. N. K. Mooers, 1977: Wind-forced continental shelf waves in the Florida Current. *J. Geophys. Res.* (in press).

Dickinson, R. E., 1968: Planetary waves propagating vertically through weak westerly wind wave guides. *J. Atmos. Sci.*, **25**, 984–1002.

Düing, W. O., C. N. K. Mooers and T. N. Lee, 1977: Low-frequency variability in the Florida Current and relations to atmospheric forcing from 1972 to 1974. *J. Mar. Res.* (to appear).

Eckart, C. H., 1960: *Hydrodynamics of Oceans and Atmospheres.* Pergammon Press, 290 pp.

——, 1962: Internal waves in the ocean. *Phys. Fluids*, **4**, 791–799.

Grimshaw, R., 1976: The stability of continental shelf waves in the presence of a boundary current shear. Res. Rep No. 431976, School of Mathematical Sciences, University of Melbourne, 19 pp.

Hamon, B. V., 1962: The spectrums of mean sea level at Sydney, Coff's Harbor and Lord Howe Island. *J. Geophys. Res.*, **67**, 5147–5155.

Keller, H. B., 1969: *Numerical Methods for Two-point Boundary Value Problems.* Blaisdell, 184 pp.

Lindzen, R. S., and H. L. Kuo, 1969: A reliable method for the numerical integration of a large class of ordinary and partial differential equations. *Mon. Wea. Rev.*, **97**, 732–734.

McKee, W. D., 1977: Continental shelf waves in the presence of a sheared geostrophic current. *Proc. IUTAM Symp. on Waves in Water of Varying Depth*, Canberra (in press).

Mooers, C. N. K., and D. A. Brooks, 1977: Fluctuations in the Florida Current, Summer 1970. *Deep-Sea Res.* (to appear).

Mysak, L. A., 1967: On the theory of continental shelf waves. *J. Mar. Res.*, **25**, 205–227.

Niiler, P. P., and L. A. Mysak, 1971: Barotropic long waves along an eastern continental shelf. *Geophys. Fluid Dyn.*, **2**, 273–288.

——, and W. S. Richardson, 1973: Seasonal variability of the Florida Current. *J. Mar. Res.*, **31**, 144–167.

Pillsbury, J. E., 1890: The Gulf Stream. Report of the U. S. Coast and Geodetic Survey for 1890, Appendix No. 10, 461–620.

Robinson, A. R., 1964: Continental shelf waves and the response of sea level to weather systems. *J. Geophys. Res.*, **69**, 367–368.

Schott, F., and W. Düing, 1976: Continental shelf waves in the Florida Straits. *J. Phys. Oceanogr.*, **6**, 451–460.

Wang, D-P., 1975: Coastal trapped waves in a baroclinic ocean. *J. Phys. Oceanogr.*, **5**, 326–333.

——, and C. N. K. Mooers, 1976: Coastal-trapped waves in a continuously stratified ocean. *J. Phys. Oceanogr.*, **6**, 853–863.